Zirconia-Based Electrolyte Stability in Direct-Carbon Fuel Cells with Molten Sb Anodes

Xiaoliang Zhou,[a,b] Tae-Sik Oh,[a,z] John M. Vohs,[a,*] and Raymond J. Gorte[a,*]

[a]*Department of Chemical and Biomolecular Engineering, University of Pennsylvania, Philadelphia, Pennsylvania 19104, USA*
[b]*Academy of Fundamental and Interdisciplinary Science, Harbin Institute of Technology (HIT), Harbin 150001, People's Republic of China*

Direct carbon fuel cells (DCFC) that use zirconia-based electrolytes and molten Sb anodes have much promise for the efficient conversion of carbonaceous solid fuels into electricity. However, etching of the electrolyte, and ultimately cell failure, has been observed during operation. In this study, we have investigated this etching phenomenon as a function of the electrolyte composition and cell operating conditions and demonstrated that it is not electrochemical in nature, but rather results from reaction between the electrolyte and Sb_2O_3 that is produced during cell operation. Etching was also observed when a yttria-stabilized zirconia (YSZ) wafer was immersed in molten Sb_2O_3.
 [DOI: 10.1149/2.0871506jes]

Manuscript submitted November 17, 2014; revised manuscript received March 5, 2015. Published March 13, 2015.

Electrical power generation in a solid oxide fuel cell (SOFC) directly utilizing solid, carbonaceous fuels (e.g. coal and biomass) would provide significant benefits including high energy conversion efficiency. CO_2 sequestration, if needed, is easy since the exhaust gas from the anode is highly concentrated.[1] Direct utilization of solid carbonaceous fuels would eliminate the need for gasification and steam reforming steps leading to great simplification of the overall system.[2]

The transfer of oxide ions from the electrolyte to the solid fuel is often found to be the limiting step for SOFCs operating on solid fuels.[3] Among various approaches to facilitate this transfer,[4–7] one of the most promising routes is to use of molten-metal electrodes.[8–10] In this scheme, the anode reaction occurs in two steps:

$$nM + xO^{2-} \rightarrow M_nO_x + 2xe^- \quad [1]$$

$$(x/2)C + M_nO_x \rightarrow (x/2)CO_2 + nM \quad [2]$$

The first step (Equation 1) is the electrochemical oxidation of some portion of the metal in the anode at the electrolyte-anode interface. The oxidized metal is then transported (via diffusion, natural convection or mechanical mixing) to access solid fuel where the carbon is oxidized while reducing metal oxide back to metal (Equation 2). Sn previously attracted much attention as the molten metal phase for this process.[8,9] Unfortunately, there is evidence that a solid SnO_2 layer forms at the electrolyte-anode interface during fuel cell operation, inhibiting further facile transfer of the oxygen from the electrolyte, resulting in high electrode losses.[11,12] While this can be avoided by using a molten metal with high oxygen solubility that does not form a stable bulk oxide phase at SOFC operating temperatures (such as Ag), electrode impedances can still be high due to slow diffusion of oxide ions within the molten metal.[13]

In our opinion, the metal that has provided the most intriguing results as an anode for this type of direct carbon fuel cell (DCFC) is Sb.[14–16] Both Sb (melting point 903 K) and Sb_2O_3 (melting point 929 K) become liquid at SOFC operation temperature ranging from 973 to 1073 K. This precludes the formation of a solid metal-oxide film at the electrolyte-anode interface as in the case of Sn. Furthermore, reduction of Sb_2O_3 by carbon is facile and has been practiced industrially for more than 100 years.[17] Although the Open-Circuit Voltage (OCV) for Sb oxidation is only 0.75 V at 973 K, the energy losses associated with this low potential are largely compensated by the very low electrode impedance that can be obtained with molten Sb electrodes, ~0.1 Ωcm^2 at 973 K.[10] This impedance is also reasonably independent of the $Sb:Sb_2O_3$ ratio.[18] Furthermore, molten-Sb electrodes are able to completely convert a large variety of solid carbon sources.[19]

However, previous work has raised questions about the long-term stability of the solid ceramic electrolytes typically used in these types of systems due to the very corrosive nature of $Sb\text{-}Sb_2O_3$ mixtures. For example, in experiments with scandia-stabilized zirconia (ScSZ), it was reported that the electrolyte became thinner by ~25 μm during the course of 200-h experiments at 973 K when the current density was 0.5 A/cm^2.[19] The rate of electrolyte thinning was strongly dependent on the current density, to such an extent that a 650-h test with a ScSZ electrolyte at 973 K and a current density of only 0.1 A/cm^2 was inconclusive in demonstrating whether or not thinning occurred. Because no thinning was reported for a 200-h test using yttria-stabilized zirconia (YSZ) as the electrolyte at with a current density of 0.5 A/cm^2, the earlier study speculated that the loss of electrolyte may depend on the identity of the rare earth dopant in the electrolyte.[19]

In the present study, we set out to understand what caused the electrolyte etching in previous work and to determine whether there are conditions under which this etching can be avoided. What we will show is that the etching phenomenon is not limited to ScSZ but also occurs with YSZ and calcia-doped zirconia (CaSZ). The etching process is not electrochemical in nature but is rather associated with reaction of antimony oxides with zirconia, a result that was confirmed in simple reaction studies of YSZ with Sb_2O_3. Differences observed between YSZ and ScSZ in a previous study are apparently caused by differences in the local concentrations of Sb_2O_3 at the electrolyte interfaces. The long-term stability in these systems will depend on finding an electrolyte that is unreactive with antimony oxides.

Experimental

Three different zirconia-based electrolyte materials were used in this study: ScSZ ($Sc_{0.1}Zr_{0.9}O_{2-\delta}$), YSZ (8 mol% Y_2O_3-92 mol% ZrO_2), and CaSZ($Ca_{0.13}Zr_{0.87}$ $O_{2-\delta}$). For each electrolyte, test cells were made by tape-casting procedures that have been described in detail elsewhere.[20] Briefly, tapes, with and without pore formers, were laminated and fired to produce a bilayer wafer of the electrolyte material with one layer porous and the other dense. For all cells, the porous layer was 50-μm thick. The dense electrolytes were 100-μm thick for cells made from ScSZ, 125-μm for cells made from YSZ, and 180-μm for cells made from CaSZ. The circular porous layer was 0.67 cm in diameter while the dense electrolyte layer was 1.4 cm in diameter. The cathodes were prepared from the porous layer by infiltration of nitrate salts to produce a composite that was 35 wt% $La_{0.8}Sr_{0.2}FeO_3$ (LSF).[21] A silver current collecting wire was attached to the cathode with silver paste and the button cells were then sealed to the end of an

*Electrochemical Society Active Member.
[z]E-mail: taeoh@seas.upenn.edu

alumina tube, with the cathode on the outside, using ceramic adhesive (Aremco, Ceramabond 552).

To form the anode, 48 grams of Sb powder (100 mesh, 99.5%, Alfa Aesar) was poured into the vertical alumina tube, with the electrolyte wafer at the bottom. This large amount of Sb was used so that the cell could be operated for longer times without requiring the addition of fuel to reduce Sb_2O_3 as it formed, as was done in past work.[10,19] The electrochemical processes at the electrolyte-anode interface (i.e. oxidation of Sb) are the same in both cases, however, so this should not affect the etching of the electrolyte. Previous work has shown that, during operation, the molten metallic Sb will remain at the bottom, in contact with the fuel cell electrolyte, while Sb_2O_3 will float to the surface of the anode.[22] For current collection at the anode, a single, 0.5-mm diameter Re wire was inserted into the molten Sb to a depth of 5 mm from the bottom. However, because Re wire corrodes in the presence of Sb_2O_3, the wire was first threaded through a 2-mm OD alumina tube to protect that part of the Re wire extending through the Sb_2O_3 layer, leaving 8 mm of Re extending past the end of the alumina tube. This exposed Re wire was bent in 90 degrees so that a portion would be suspended parallel to the cell. The end of the 2-mm tube was then sealed with ceramic adhesive (Aremco, Ceramabond 552) to prevent Sb from entering. Finally, glass wool was added to the open top of the alumina tube to minimize the reaction of gas-phase O_2 with the Sb and the tube containing the cell was inserted into a tube furnace. All electrochemical measurements in this study were performed at 1023 K.

A Gamry Instruments Potentiostat was used to measure V-i polarization curves and impedance spectra. It was also used to maintain a constant potential across the cell during discharge and to integrate the current over time to determine the amount of charge that passed through the electrolyte. Current densities were calculated based on the projected area of the cathode. The performance characteristics of the cells in this study were similar to those described in previous studies,[10,19] demonstrating that using large amounts of Sb did not affect performance. The OCVs were always 0.72 V at 1023 K, in close agreement with that expected for the oxidation reaction of Sb to Sb_2O_3. The V-i polarization relationships were nearly linear, and the non-ohmic contributions to the impedance spectra were consistently less than 0.2 Ωcm^2, at least for cells with YSZ or ScSZ electrolytes. However, because we were only able to use a single lead for electrical connection to the molten anode in the present experiments, there was an added ohmic contribution of 0.6 to 0.8 Ωcm^2 in all impedance spectra due to the lead wire. This in turn cause the observed voltages for a given current density to be lower here than in previous work.[10,19]

After operation, selected cells were cut in half, mounted on an epoxy mold, and polished to facilitate analysis of the structural changes that occurred in the electrolyte during discharge. Cross sectional images were collected by either JEOL-7500F scanning electron microscope (SEM) or optical microscope.

To determine whether etching of YSZ would occur in the presence of Sb_2O_3, in the absence of a fuel cell, we vertically placed a 118-μm thick YSZ wafer in a 13-cm^3 alumina crucible together with 7.5 g of Sb and 6.5 g of Sb_2O_3. This was then covered and heated to 1073 K for 35 h. After cooling to room temperature, the crucible was sliced open and the YSZ wafer was examined in the optical microscope.

Results and Discussion

To determine the stability of the molten-Sb fuel cells, experiments were performed in which the cell potential was maintained at 0.2 V while monitoring the current density as a function of time. The results of one such experiment are shown in Fig. 1 for a cell with a ScSZ electrolyte. The cell initially exhibited a current density of 0.52 A/cm^2, and a total resistance of 1.0 Ωcm^2, as determined by the slope of the linear polarization curve. Most of this resistance is attributable to the Re electrical lead. Similar to what was reported in previous long-term experiments,[19] we observed an initial small decrease in performance, followed by a small but steady increase in current density with time up to approximately 80 h, after which the current dropped rapidly to zero. Since the amount of charge that had been drawn after 80 h was 69,000 C, corresponding to an amount of oxygen that would oxidize only 29 g of Sb to Sb_2O_3, the cell failure at the end of the experiment was not due to complete consumption of the metal. Indeed, when the cell was cooled and cut in half, several centimeters of metallic Sb remained at the bottom of the cell, below several centimeters of Sb_2O_3. (These layers were easily distinguished by their appearance, as shown in our previous work.[19,22]) Rather, the abrupt loss in cell performance in Figure 1 was due to failure of the electrolyte.

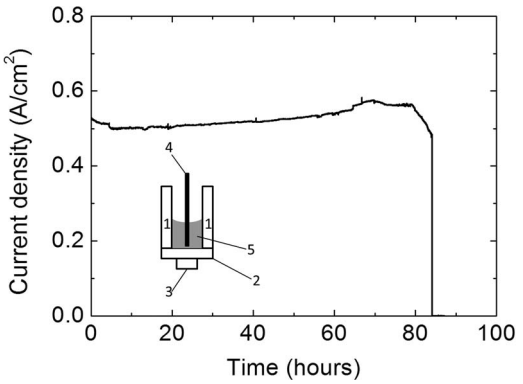

Figure 1. Current density as a function of time for an upright cell with ScSZ electrolyte operated at 0.2 V and 750°C. The inset depicts the cell configuration. 1: alumina tube, 2: ScSZ electrolyte, 3: ScSZ-LSF cathode, 4: Re wire current collector, 5: Molten Sb/Sb oxide mixture.

Figure 2 shows cross-sectional SEM images of this same cell at various magnifications. Figure 2a is a schematic of the cell, with Figures 2b to 2d providing micrographs with increasing magnification of the indicated areas. Red dashed lines have been added to the SEM

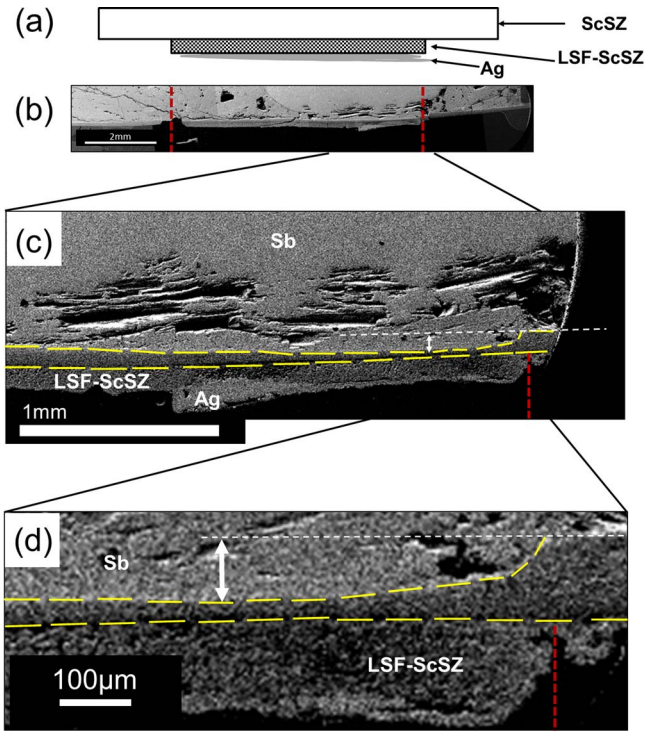

Figure 2. (a) Schematic view of the upright ScSZ cell in Figure 1. (b) Post-operation cross-sectional image of the cell. (c), (d) Zoomed-in views at two different magnifications of regions where etching occurred. Vertical dotted red lines denote the end position of cathode. Yellow broken lines mark the electrolyte-electrode interfaces after operation, while the white dotted lines and double-headed arrows show how thickness change was measured.

Table I. Experimental conditions for 7 upright cells.

	Electrolyte	Voltage (V)	Current density (A/cm^2)	Charge (1000 C)	$-\Delta t$ (μm)
1	ScSZ	0.2	0.5	69	88
2	ScSZ	0.2	0.2	32	35
3	ScSZ	0.5	0.35	76	103
4	CaSZ	0.2	0.12	10.5	40
5	YSZ	0.2	0.4	7.2	50
6	YSZ	0.35	0.3	3.6	30
7	YSZ	0.5	0.2	15.8	102

images to show where the cathode layer ends. These data demonstrate that there was severe thinning of the electrolyte, as reported previously.[19] This thinning was not uniform over the entire cell since there was no evidence for thinning in regions beyond the edge of the cathode. There was also minimal thinning of the electrolyte in the center of the cell. However, near the edge of the cathode, the etching was very severe, with the ScSZ electrolyte having decreased to less than 25% of its original thickness. Notice that the thinning observed in Figure 2 is sufficient to explain the increasing current density with time in Figure 1.

We considered the possibility that the electrolyte etching observed in Figure 2 is dependent on the cell operating potential, current density, or the use of Sc as dopant in the zirconia. Table I provides results from experiments similar to those reported in Figure 1 and 2 but performed with different electrolytes and different cell potentials. Because ohmic resistances of the lead wires were somewhat variable, the current densities for a given cell potential were not the same from cell to cell. In each experiment, the current density was nearly constant until the cell failed; these nominal current densities are shown in the fourth column of the table, while the total charge that had passed through the electrolyte before failure are given in the fifth column. Etching of the electrolyte was observed in all of the cells and the maximum amounts of thinning, $-\Delta t$, are listed in column 6. Although there was variability in the level of thinning observed, it is readily apparent from Table I that etching occurred in all of the cells, independent of cell potential or current density. Etching, at least in the present study, was more severe with YSZ and CaSZ than with ScSZ. The cell potential also did not appear to be a factor, since cells operated at 0.5 V etched as much as those operated at higher overpotentials.

In these experiments, natural convection is the primary method for transporting Sb_2O_3 away from the electrolyte due to its density difference from metallic Sb. Therefore, we also examined the performance of a cell inclined 55 degrees from the vertical axis in order to change the natural-convection flow pattern. We chose to test a cell with a YSZ electrolyte at a constant cell potential of 0.35 V. The current density as a function of time for this experiment is shown in Figure 3. Unlike what was observed in Figure 1, the current density did not increase with time but remained nearly constant at 0.26 A/cm^2 for more than 135 h, corresponding to a passed charge of 45,000 C. This cell was able to operate much longer, and at a more stable current density, than was observed for the other YSZ cells in Table I that were operated vertically.

Optical, cross-sectional images for this cell following the test period are shown in Fig. 4. The top picture, Figure 4a, shows the entire cell, with red lines to mark the edges of the cathode. Higher magnification pictures of the regions near the edge of the cathode are reported in Figure 4b and 4c, with Figure 4b showing edge at the lowest point of the inclined cell and Figure 4c the edge at the top. What is most interesting is that there is minimal thinning of the electrolyte in most parts of the cell, including especially at the bottom cathode edge. Electrolyte thinning was localized mainly to the top end of the cell, near the edge of the cathode. In this narrow region, the etching was severe and the electrolyte had thinned by more than half.

These results are inconsistent with electrolyte etching being an electrochemical process since the etching would then be expected to occur uniformly over the electrolyte. However, the results can be understood by assuming that Sb_2O_3 can react with zirconia-based electrolytes. First, the fact that the OCV of fuel cells operating on molten Sb are well defined and invariant with the extent of Sb conversion demonstrates that Sb and Sb_2O_3 must form separate phases under fuel cell conditions. If oxygen were merely soluble in the molten metal, the OCV would vary with the amount of oxygen. A variable OCV is observed in cells operating on molten Pb[14] and molten Ag[13] but not with molten Sb.[10,19] Second, the large difference in densities between Sb (6.7 g/cm^3) and Sb_2O_3 (5.2 g/cm^3) implies that natural convection will be important in this system. Figure 5 shows the flow patterns that are expected for natural convection with horizontal and inclined heated plates. For the inclined cell, there should be a much higher concentration of Sb_2O_3 near the top than at the bottom. Similarly, one should expect the oxide concentration to be maximized near the outside edges with the horizontal cell. These are the positions of maximal etching in the cells.

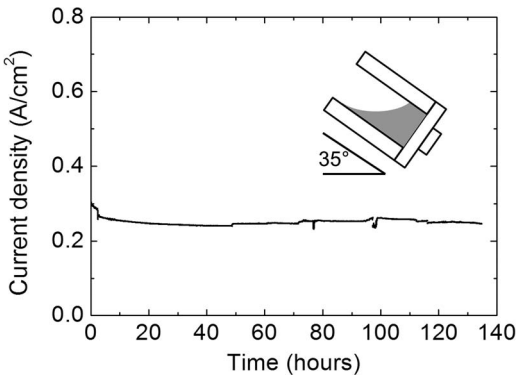

Figure 3. Long term current density behavior of a tilted cell with YSZ electrolyte at 0.35 V. Operation temperature is 750°C. The inset shows the tilting angle.

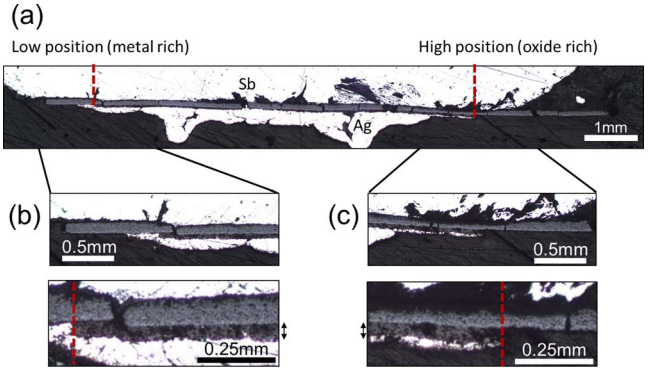

Figure 4. (a) Post-operation cross-sectional image of the tilted YSZ cell in Figure 3. Vertical dotted red lines denote the end positions of cathode. (b) Zoomed-in view on region of minimal etching. (c) Zoomed-in view on region of severe etching at the top. Bottom figures for (b) and (c) show the composite cathode layers with double-headed arrows marking their thickness.

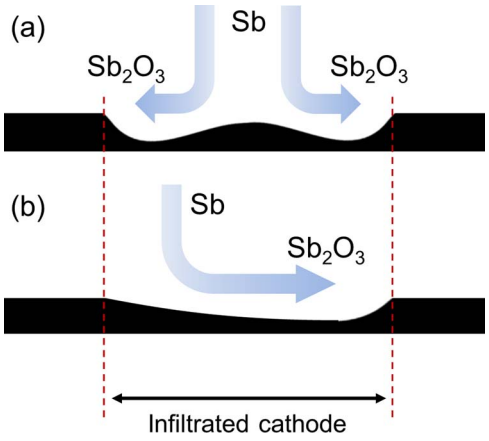

Figure 5. Etch front schematics for (a) upright cells, and (b) tilted cells. For tilted cells, metal rich side is on the left (lower position) whereas oxide rich side is on the right (higher position).

To determine whether etching would occur when YSZ was placed in the presence of Sb_2O_3 without any electrochemical reaction, we examined the YSZ that was placed vertically in the alumina crucible containing Sb and Sb_2O_3. After heating to 1073 K for 35 h, the crucible was cut open and the YSZ wafer examined. At the end of the experiment, the top layer of the Sb-containing bed was solid Sb_2O_4, apparently formed by reaction of the Sb_2O_3 with air leaking into the crucible. The bottom of the crucible still contained a large of amount of metallic Sb and there was a well-defined middle region of Sb_2O_3, identifiable by a difference in color and XRD pattern. The YSZ wafer extended through the different layers. In the Sb_2O_3 region, it had thinned from 118 μm to 94 μm, demonstrating that etching could occur without current flow.

Exactly why Sb_2O_3 causes thinning of the zirconia-based electrolytes is uncertain. We are not aware of compounds forming between Sb_2O_3 and ZrO_2, although Sb_2O_3 does form mixed-metal oxides with CaO and many other metal oxides. Attempts to observe a reaction between Sb_2O_3 with YSZ by heating powder mixtures did not result in any new products observable by X-Ray diffraction. In our previous work, energy-dispersive X-ray spectroscopy (EDS) did not reveal the location of the Zr atoms in Sb/Sb oxide.[19] It is currently an open question where the etched-out mass goes. Zr containing compounds can possibly be precipitating out from the molten phase even though it is very hard to detect them. To explain why the etching is so localized to the vicinity of the electrode, we propose that there may be a modest solubility of zirconia in the molten Sb_2O_3 phase, so that convective flows would be required to move the "dissolved" oxide from the surface.

Previous reports that etching may be different depending on the dopant used to stabilize zirconia are likely due to difficulties in reproducing the exact same conditions from cell to cell.[19] For example, it is very likely that the Sb_2O_3:Sb ratio varied from cell to cell in the earlier study due to the fact that it is difficult to add solid fuels to the cell in a reproducible manner. In the present study, etching was clearly observed for Sc, Y, and Ca dopants.

Obviously, it would not be practical to operate a fuel cell with the electrolyte instability observed in this study. It has been suggested that doped ceria electrolytes could offer stable operation[23] but sufficiently long-term testing has not yet been done to verify whether these electrolytes would be sufficiently stable for practical applications. Given the great promise of this technology for the efficient utilization of solid carbon fuels, it seems that a search for stable materials is needed.

Conclusions

Thinning of zirconia-based electrolytes in SOFC with molten Sb anodes is due to chemical reactions between Sb_2O_3 and the zirconia. It appears that ZrO_2 has some limited solubility in the molten Sb_2O_3 and that flow of the Sb_2O_3 due to natural convection is responsible for slow loss of the electrolytes.

Acknowledgments

The authors thank the U.S. National Science Foundation for financial support for this research project (grant no. DMR-1210388). X.Z. also acknowledges financial support from the Natural Science Foundation of China (No. 21106025) and the Open Project of State Key Laboratory of Urban Water Resource and Environment, Harbin Institute of Technology (No. QA201113).

References

1. D. X. Cao, Y. Sun, and G. L. Wang, *J. Power Sources*, **167**, 250 (2007).
2. S. Li, A. C. Lee, R. E. Mitchell, and T. M. Gür, *Solid State Ionics*, **172**, 1549 (2008).
3. S. Nürnberger, R. Bußar, P. Desclaux, B. Franke, M. Rzepka, and U. Stimming, *Energy Environ. Sci.*, **3**, 150 (2010).
4. A. S. Lipilin, I. I. Balachov, L. H. Dubois, A. M. C. Sanjurjo McKubre, S. Crouch-Baker, M. D. Hornbostel, and F. L. Tanzella, US Pat. 8,01,310 (2012).
5. Y. Nabae, K. D. Pointon, and J. T. S. Irvine, *Energy Environ. Sci.*, **1**, 148 (2008).
6. S. L. Jain, J. B. Lakeman, K. D. Pointon, R. Marshall, and J. T. S. Irvine, *Energy Environ. Sci.*, **2**, 687 (2009).
7. A. C. Lee, S. Li, R. E. Mitchell, and T. M. Gür, *Electrochem. Solid-State Lett.*, **11**, B20 (2008).
8. T. Tao, L. Bateman, J. Bentley, and M. Slaney, *ECS Trans.*, **5**, 463 (2007).
9. T. Tao, M. Slaney, L. Bateman, and J. Bentley, *ECS Trans.*, **7**, 1389 (2007).
10. A. Jayakumar, R. Küngas, S. Roy, A. Javadekar, J. M. Vohs, D. J. Buttrey, and R. J. Gorte, *Energy Environ. Sci.*, **4**, 4133 (2011).
11. A. Jayakumar A, S. Lee, A. Hornes, J. M. Vohs, and R. J. Gorte, *J. Electrochem. Soc.*, **157**(3), B365 (2010).
12. H. Wang, Y. Shi, and N. Cai, *J. Power Sources*, **246**, 204 (2014).
13. A. Javadekar, A. Jayakumar, R. Pujara, J. M. Vohs, and R. J. Gorte, *J. Power Sources*, **214**, 239 (2012).
14. A. Jayakumar, J. M. Vohs, and R. J. Gorte, *Ind. Eng. Chem. Res.*, **49**(21), 10237 (2010).
15. H. Wang, T. Cao, Y. Shi, N. Cai, and W. Yuan, *Energy*, **75**, 555 (2014).
16. Y. Cao, H. Wang, Y. Shi, and N. Cai, *Fuel*, **135**, 223 (2014).
17. J. A. DeCew, in *Metallurgical and Chemical Engineering*, ed. E. F. Roeber and H. C. Parmelee, p. 444, McGraw-Hill Publishing Co Inc., New York (1917).
18. A. Javadekar, A. Jayakumar, R. J. Gorte, J. M. Vohs, and D. J. Buttrey, *J. Electrochem. Soc.*, **159**(4), A386 (2012).
19. A. Jayakumar, A. Javadekar, J. Gissinger, J. M. Vohs, G. W. Huber, and R. J. Gorte, *AIChE J.*, **59**, 3342 (2013).
20. J. M. Vohs and R. J. Gorte, *Adv. Mater.*, **21**, 943 (2009).
21. T.-S. Oh, A. S. Yu, L. Adijanto, R. J. Gorte, and J. M. Vohs, *J. Power Sources*, **262**, 207 (2014).
22. A. Javadekar, A. Jayakumar, R. J. Gorte, J. M. Vohs, and D. J. Buttrey, *J. Electrochem. Soc.*, **158**(12), B1472 (2011).
23. X Xu, W. Zhou, and Z. Zhu, *Ind. Eng. Chem. Res.*, **52**, 17927 (2013).